Journal of Analytical and Applied Pyrolysis 115 (2015) 132–142

Contents lists available at ScienceDirect

Journal of Analytical and Applied Pyrolysis

journal homepage: www.elsevier.com/locate/jaap

TGA/DTA–FTIR–MS coupling as analytical tool for confirming inclusion complexes occurrence in supramolecular host–guest architectures

Cristian-Dragos Varganici [a], Narcisa Marangoci [a], Liliana Rosu [a], Cristian Barbu-Mic [b,c], Dan Rosu [a,*], Mariana Pinteala [a], Bogdan C. Simionescu [a,b,c]

[a] Centre of Advanced Research in Bionanoconjugates and Biopolymers, "Petru Poni" Institute of Macromolecular Chemistry, 41A Gigore Ghica-Voda Alley, 700487 Iasi, Romania
[b] "Petru Poni" Institute of Macromolecular Chemistry, 41A Gigore Ghica-Voda Alley, 700487 Iasi, Romania
[c] Department of Natural and Synthetic Polymers, "Gh. Asachi" Technical University of Iasi, 73 Dimitrie Mangeron Boulevard, 700050 Iasi, Romania

ARTICLE INFO

Article history:
Received 3 April 2015
Received in revised form 1 July 2015
Accepted 10 July 2015
Available online 16 July 2015

Keywords:
Viologen
Rotaxane
Thermal decomposition kinetics
Evolved gas analysis

ABSTRACT

The paper deals with the insights on the thermal decomposition of a viologen included in a [2]rotaxane structure alongside β-cyclodextrin. Thermal stability studies were conducted by dynamic thermogravimetry in inert atmosphere. Complexation phenomena occurence led to an increase in inclusion complex thermal stability. Simultaneous TGA–DTA analysis indicated lower intensity of the complexed guest molecule melting profile. Kinetics of the thermal decomposition process was conducted by applying the isoconversional methods of Friedman and Flynn–Wall–Ozawa. Global kinetic parameters values exhibited an increase with the conversion degree, indicating a complex thermal degradation process. The form of the kinetic model which best described the thermal decomposition process and the kinetic parameters values corresponding to each degradation stage were determined with a multivariate non-linear regression method. A two dimensional diffusion (D2) kinetic model best fitted the thermogravimetric data. A correlation between kinetic data and structural changes during thermal decomposition was established. The evolved gas analysis was conducted on a coupling of simultaneous thermal analysis device to a quadrupole mass spectrometer and a Fourier transform infrared spectrophotometer. The complex gaseous mixture evolved during thermal decomposition of the structure was comprised of: water, carbon monoxide, carbon dioxide, hydrogen cyanide, methanol and ethanol, acetic acid, hydrogen bromide and amine and furan derivatives.

1. Introduction

One main feature of 4,4-bipyridine resides in its property to form diquaternary salts regarded to as viologens. Their name was attributed on the basis of their color changing when exposed to a series of physical factors (e.g. light). The scientific interest of such salts grew due to some specific applications including electron carriers, pro-oxidants for oxidative stress testing, cardiovascular agents, herbicides, neuromuscular and hypotensive agents, molecular wires in electronic devices, electrochromic display devices [1,2]. Viologens also exhibit antibacterial efficiency against some microorganism species [3], such as *Escherichia coli*, due to their DNA strand scission ability [4]. Michaelis first exploited viologens' electrochemical properties in 1933 [5]. Due to their low redox potential and the toxic effect on mammals [6], viologens aroused suspicions regarding their toxicity on the human organism and thus many works were reported on evaluating their action, for example those undertaken for methyl viologen (Paraquat) herbicide [7,8]. In a work by Hatcher and co-authors [9] there is even reported an increase in Parkinson's disease because of some viologen herbicides. After ingestion, 4,4′-bipyridyl viologens (Bpy^{2+}) undergo an enzymatic reduction mechanism during which there is generated a radical cation ($Bpy^{\bullet+}$). This cation, in the presence of O_2 and/or H_2O_2, further produces extremely reactive radicals, such as $HO^{\bullet}$. This leads to the oxidation of biochemical important entities, such as lipid membranes, proteins and nucleic acids [2,10]. In this sense, current research in the domain is focused on the reduction of viologens toxicity and thus to exploit their redox potential for pharmacological interest. One such method, already published by our group, consists in incorporating viologens, through different procedures, in β-cyclodextrin (βCD), forming host–guest inclusion complexes [2].

* Corresponding author. Tel.: +40 232 217 454; fax: +40 232 211 299.
E-mail addresses: drosu@icmpp.ro, dan_rosu50@yahoo.com (D. Rosu).

http://dx.doi.org/10.1016/j.jaap.2015.07.006
0165-2370/

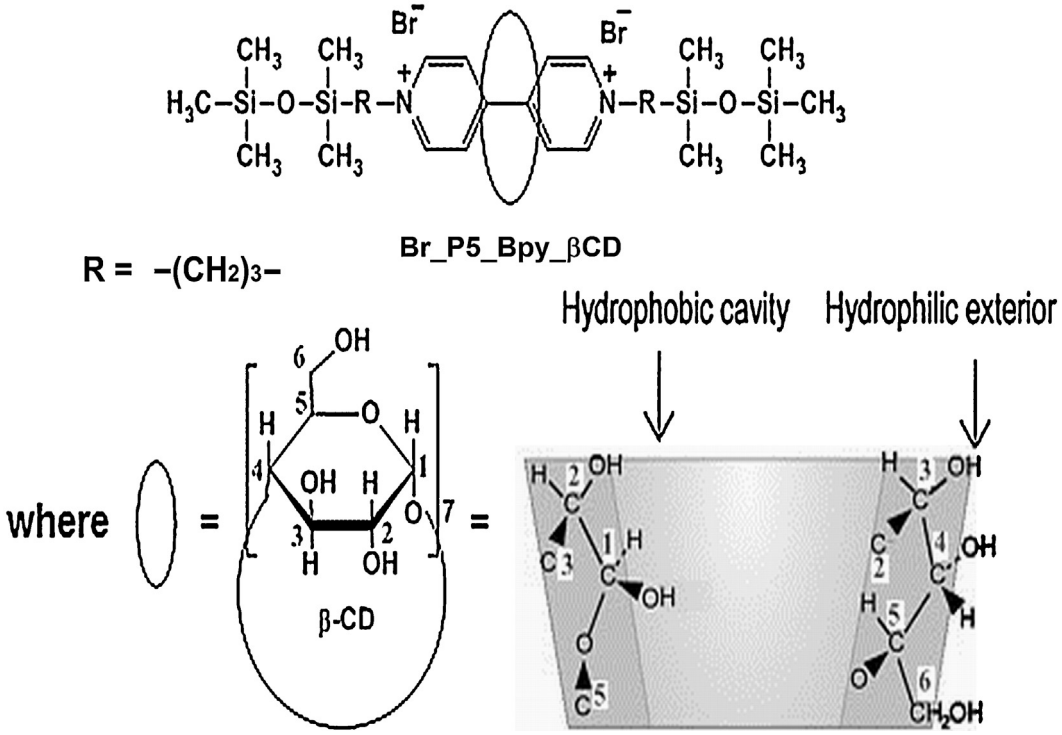

Scheme 1. Structures of the studied compounds.

Cyclodextrins are a class of oligosaccharides comprised of macrocycles of six (αCD), seven (βCD) and eight (γCD) glucopyranose units bonded through α-1,4-glycosidic linkages. Cyclodextrins possess the capacity to form inclusion complexes with different guest molecules by introducing them into their hydrophobic cavities. Through complexation, the physical, chemical and biological properties of the guest molecules are modified, representing very efficient drug carriers in controlled drug release. Cyclodextrins may, also, form inclusion complexes with rotaxane and/or pseudorotaxane structures [2,11].

Due to their unique features, such as low toxicity, oxidative stability, antiadhesive properties, physiological inertness, etc., polymethyldisiloxanes are used in a wide variety of biomedical applications (i.e. drug-delivery systems, production of artificial skin, transdermal therapeutic systems, contact lenses, etc.) [12]. Short chain siloxane end-unit entities (e.g. 1,1,3,3,3-pentamethyldisiloxane, PMDS) possess antislipping effects relative to βCD macrocycle and enhance inclusion complex biostability by decreasing its decomposition rate in the body [2,13].

Since authors recently reported the obtaining of a supramolecular architecture based on a viologen included in a [2]rotaxane structure alongside βCD [2], no other previous attempt to study its thermal decomposition behavior and evolved gas analysis has been undertaken. This study is interesting from both theoretical point of view, for gaining new knowledge on the thermal behavior of such supramolecular architectures, and from a potentially practical point of view, since the establishment of an accurate thermal decomposition mechanism may play an important role in the industrial processing of the future drug.

Recent studies on isoconversional kinetic methods applied in the thermal decomposition of supramolecular cyclodextrin based inclusion complexes were also described in the literature [14,15]. However, to our knowledge, none such studies were reported to this point on rotaxane and cyclodextrin supramolecular architectures. The closest kinetic approach to our study was undertaken by Zhang et al. [16] which studied dissociation kinetics of βCD-ethyl benzoate under isothermal and non-isothermal conditions and also found a thermal decomposition mechanism best described by diffusion models.

2. Materials and methods

2.1. Synthesis

The synthesis, structural characterization and toxicological assessment of a β-cyclodextrin-caged 4,4′-bipyridinium-bis(siloxane) inclusion complex ([2]{[1][(1,1′-di(propyl-3-pentamethyldisiloxane)-4,4′-bipyridinium]-*rotaxa*-[β-cyclodextrin]} according to IUPAC nomenclature), as a potential pharmaceutical candidate, were described in a previous paper. According to the authors, the synthesis pathway was comprised of two stages: (i) formation of the inclusion complex of βCD and 4,4′-bipyridine (BPy), through coprecipitation, and (ii) quaternization of nitrogen atoms of caged 4,4′-bipyridine, via the bromide atom of the presynthesized 1-(3-bromopropyl)-pentamethyldisiloxane [2]. The studied structure is depicted in Scheme 1.

2.2. Measurements

The thermal decomposition and evolved gas analysis were performed on a TGA–FTIR–MS system, equipped with a device of simultaneous TGA/DTA analysis STA 449F1 Jupiter model (Netzsch, Germany), FTIR spectrophotometer Vertex-70 model (Bruker, Germany) and a mass spectrometer QMS 403C Aëolos model (Netzsch, Germany). The TG/DTA thermobalance was coupled online with FTIR spectrophotometer and mass spectrometer through two heated transfer lines. 10 mg of each sample was heated from 30 to 700 °C under nitrogen flow (flow rate 50 mL min^{-1}), in an open Al_2O_3 crucible and Al_2O_3 as reference material was used. Heating rates of 10, 20, 30 and 40 °C min^{-1} were applied. The transfer line to FTIR spectrophotometer was made of polytetrafluorethylene, had an interior diameter of 1.5 mm and was heated at 290 °C.

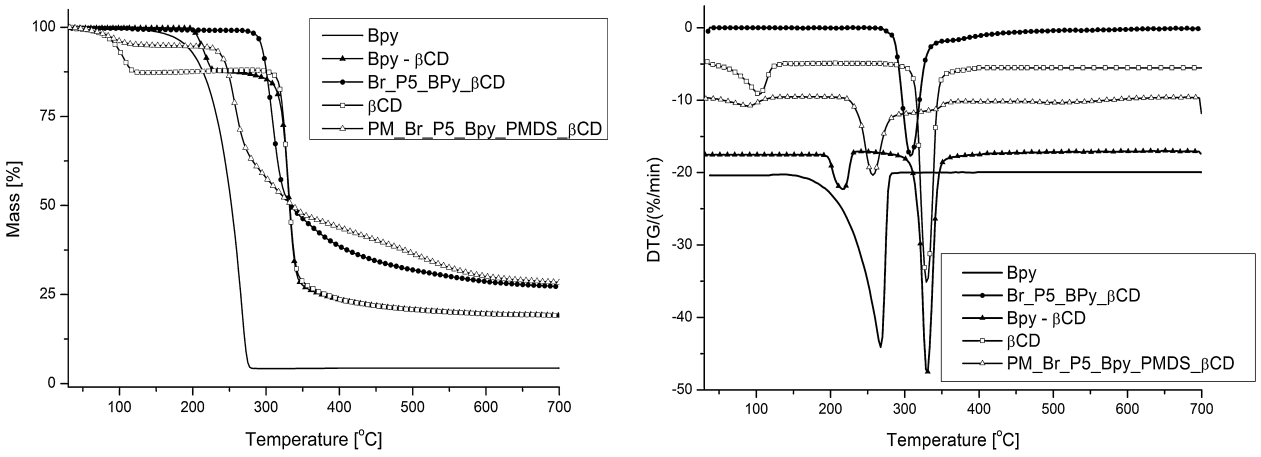

Fig. 1. TGA and DTG curves of the studied structures.

The spectra were acquired with a spectral resolution of 4 cm^{-1} on 400–4000 cm^{-1} range. The transfer line to MS spectrometer QMS 403C is made of a quartz capillary with an internal diameter of 75 μm and was heated at 290 °C. The mass spectra were recorded under electron ionization energy of 70 eV. Data were scanned in the range m/z = 1–300, the measuring time for each cycle was 150 s. The NIST Mass Spectral Database was used for the identification of ion fragments (m/z) in MS spectra. The kinetic analysis of thermogravimetric data was performed using the soft Netzsch Thermokinetic 3.

3. Results and discussion

3.1. Complexation phenomena occurrence via thermal behavior

3.1.1. Complexation demonstrated via thermal decomposition behavior

Inclusion complex formation occurs through establishment of hydrogen bonding between interior hydrogen atoms of the host molecule cavity (i.e. βCD) and the guest molecule (i.e. Bpy). In the ^{1}H NMR spectrum complexation phenomenon is usually evidenced by upfield shifting of the proton signals from third and fifth positions in the host molecule (Scheme 1) [17]. Complexation led to a significant decrease of the siloxane endcapped bipyridinium salt toxicity [2]. Thermal characterization methods, such as thermogravimetric analysis (TGA) and differential scanning calorimetry (DSC) or differential thermal analysis (DTA), are useful tools in establishing host–guest solid state interactions, which are identified by differentiating between pure substances and inclusion compounds from phase transformations occurring during heating [18]. Inclusion complex formation is generally evidenced by differences in the thermal decomposition pattern of pure guest and complexed guest molecule. Complexation is indicated by an increase in the thermal stability of the complexed guest as compared to that of the uncomplexed components. Also, the melting profile of the guest molecule in the inclusion complex gradually lowers in its intensity [19]. Fig. 1 shows the TGA thermograms and their corresponding first derivative (DTG) curves of pure 4,4′-bipyridine (Bpy) and β-cyclodextrin (βCD), complexed Bpy (Bpy–βCD), complexed siloxane endcapped Bpy (Br_P5_Bpy_βCD—Scheme 1) and the physical mixture of βCD with uncomplexed rotaxane (Br_P5_Bpy_PMDS), noted as PM_Br_P5_Bpy_PMDS_βCD. The ratio of components in the physical mixture was the same as the one used in the reported synthesis of the complex Br_P5_Bpy_βCD [2]. Fig. 2 shows the DTA thermograms of the studied structures, recorded simultaneously with the TGA ones. The extracted thermogravimetric data from Fig. 1 is given in Table 1. The temperature corresponding to 5% mass loss ($T_{5\%}$) was chosen as criterion for evaluating thermal stability of the studied structures.

As one may observe from Fig. 1 and Table 1, pure Bpy starts gradually decomposing around 190 °C in a single stage, with a mass loss of 95% and a residue value of 4.33%. Fig. 2 shows that thermal decomposition of Bpy is accompanied by a wide endothermic process, in the range 192–315 °C, with a peak value at 273 °C and an enthalpy value of 332 J g^{-1}. This aspect is due to overlapping of boiling (point around 305 °C) and thermal decomposition processes, being in good agreement with literature data [1,20]. After

Table 1
Thermal decomposition parameters extracted from thermogravimetric data.

Sample code	Stage	$T_{5\%}$ (°C)	T_{max1} (°C)	m_1 (%)	T_{max2} (°C)	m_2 (%)	T_{max3} (°C)	m_3 (%)	T_{max4} (%)	m_4 (%)	T_{endset} (°C)	W (%)
Bpy	I	190	267	95	–	–	–	–	–	–	278	4.33
Bpy–βCD	I	215	218	12	–	–	–	–	–	–	–	
	II	–	–	–	331	66	–	–	–	–	455	19
Br_P5_Bpy_βCD	I	295	308	65	–	–	–	–	–	–	350	27
βCD	I	95	104	12	–	–	–	–	–	–	–	
	II	–	–	–	331	67	–	–	–	–	455	19
PM_Br_P5_Bpy_PMDS_βCD	I	135	89	5	–	–	–	–	–	–	–	
	II	–	–	–	257	30	–	–	–	–	–	
	III	–	–	–	–	–	345	17	–	–	–	
	IV	–	–	–	–	–	–	–	509	20	577	28

$T_{5\%}$—temperature corresponding to 5% structural mass loss characterizing the first thermal decomposition stage; T_{max1}, T_{max2}—temperatures corresponding to the maximum thermal decomposition rates (DTG curve peaks) for the first and second stage; T_{endset}—thermal decomposition temperature after which no significant mass changes occur; m_1, m_2, m_3, m_4—mass loss values corresponding to each thermal decomposition stage; W—residue mass remained at the end of thermal decomposition (700 °C).

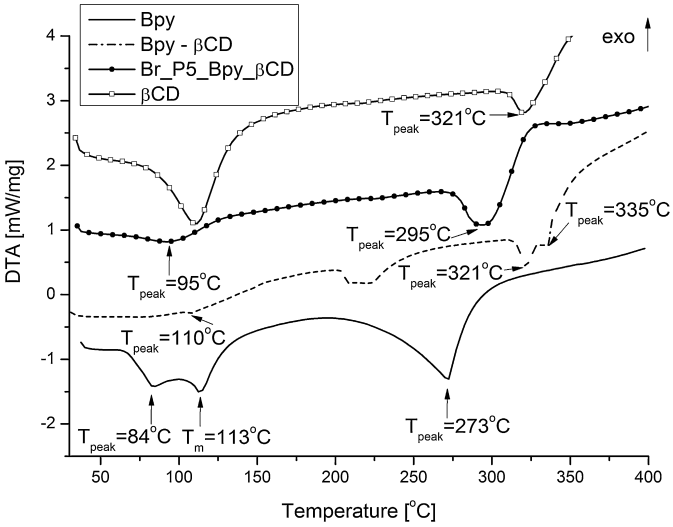

Fig. 2. DTA curves of the studied structures.

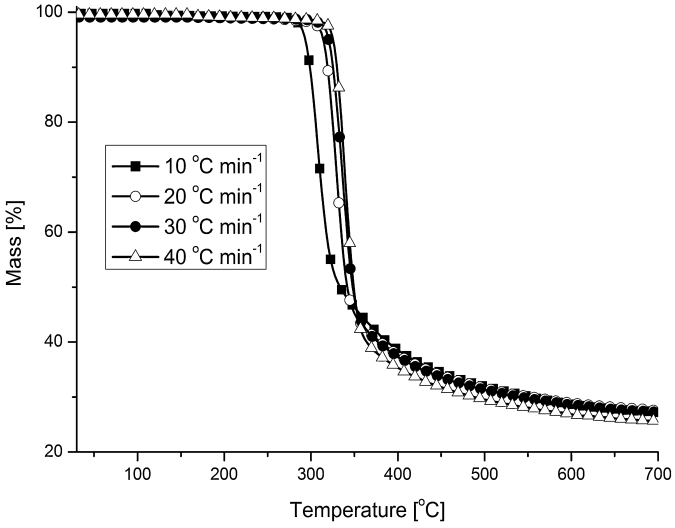

Fig. 3. Weight loss at different heating rates for sample Br_P5_Bpy_βCD.

inclusion in the βCD cavity the thermal stability of Bpy molecule increases, from 190 °C to 215 °C [19]. This aspect is further reflected by a significant increase in residual mass of Bpy–βCD (19%) compared to that of pure Bpy (4.33%). Another sign of inclusion complex formation consists in the significantly lower mass loss of the complexed guest molecule in Bpy–βCD (12%) compared to that of pure Bpy (95%) [1,20]. The host molecule cavity protects the guest molecule. The 66% mass loss in the second stage of Bpy–βCD decomposition is attributed to βCD thermal degradation, at around 310 °C [19], together with the entrapped remaining complexed drug. According to the literature, βCD thermal decomposition process is initiated by opening of the cyclodextrin rings, afterwards following a degradation pattern similar to that of cellulose by loss of the glucosidic structure and hydroxyl groups with formation of unsaturated moieties, such as carbonyl groups and aromatic structures [21]. The TGA thermogram of pure βCD indicates a 12% mass loss in the first stage, corresponding to removal of crystallized water molecules from its cavity (Fig. 1 and Table 1). The thermogram of the Bpy–βCD complex shows no water loss in the same temperature range, this also being an indication of inclusion complex formation, the guest molecule replacing the crystallized water molecules in the βCD cavity during synthesis. Furthermore, the DTA thermograms in Fig. 2 clearly show that, in the case of Bpy–βCD inclusion complex, the wide endothermic process corresponding to pure Bpy degradation is significantly reduced in intensity (25 J g^{-1} compared to 332 J g^{-1}) and seemingly shifted toward a much higher temperature domain (321 °C), its profile almost coinciding with that of pure βCD (321 °C, 20 J g^{-1}). The sole exception resides in the enthalpy values differences and the two peaked endothermic profile specific to Bpy–βCD (321 °C and 335 °C) due to simultaneous volatilization of complexed Bpy at a higher temperature domain. After endcapping Bpy–βCD with the siloxane entities, a seemingly higher thermal stability may be observed for the final product (Br_P5_Bpy_βCD) ($T_{5\%}$ = 295 °C) compared to that of pure Bpy ($T_{5\%}$ = 190 °C) and Bpy–βCD ($T_{5\%}$ = 215 °C) with a lower total mass loss (65%) and higher residue mass (27%) (Table 1). The thermal decomposition process of sample Br_P5_Bpy_βCD may overlap with that of the alkyl siloxane blockers within its structure, which occurs below 300 °C [22]. This may contribute to slightly accelerating the thermal degradation of βCD from Br_P5_Bpy_βCD ($T_{5\%}$ = 295 °C) compared to pure βCD (310 °C) (Fig. 1 and Table 1).

By analyzing Fig. 1 and Table 1, one may observe significant differences between the thermograms of the physical mixture PM_Br_P5_Bpy_PMDS_βCD and of the complex Br_P5_Bpy_βCD. The thermogram of PM_Br_P5_Bpy_PMDS_βCD characterizes a multicomponent system which thermally decomposes in four stages, corresponding to: water loss (T_{max1} = 89 °C), Bpy degradation (T_{max2} = 257 °C) and overlapping of βCD and Br-PMDS (siloxane compound) decomposition processes (T_{max3} = 345 °C and T_{max4} = 509 °C).

On the other hand, the complex Br_P5_Bpy_βCD behaves as a single system, thermally decomposing in one stage and at a superior temperature compared to the physical mixture (Fig. 1, Table 1).

3.1.2. Complexation via DTA analysis

The DTA curve of the guest compound (Bpy) exhibits a two peak endothermic profile attributed to thermal history elimination (84 °C) and Bpy melting point (T_m = 113 °C) (Fig. 2). By analyzing the DTA curve of sample Bpy–βCD one may observe that the two endothermic peaks of the guest molecule occur in a single peak with a smaller intensity and shifted toward lower temperature domains (110 °C). This is an indication of a new solid phase formation [23–25]. Inclusion complex Br_P5_Bpy_βCD also exhibits a less intense melting profile shifted toward an even lower temperature domain (T_m = 95 °C) compared to that of pure Bpy (T_m = 113 °C), this being also an indication of inclusion complex formation, as previously discussed.

3.2. Thermal decomposition kinetics

For kinetic study TGA curves at four different heating rates (10 °C min^{-1}, 20 °C min^{-1}, 30 °C min^{-1} and 40 °C min^{-1}) were recorded for sample Br_P5_Bpy_βCD as shown in Fig. 3.

Kinetic parameters were evaluated from non-isothermal experiments. The conversion degree (α) was calculated using Eq. (1), where m_i, m_t and m_f represent sample mass before degradation, at a time t, and after complete degradation.

$$\alpha = \frac{m_i - m_t}{m_i - m_f} \quad (1)$$

The conversion rate is described by Eq. (2), where t is time (min), A is the pre-exponential factor (s^{-1}), E is the activation energy of thermal decomposition (kJ mol^{-1}), R is the gas constant (8.314 kJ mol^{-1}), T is temperature (K) and $f(\alpha)$ is the conversion function.

$$\frac{d\alpha}{dt} = Ae^{-(E/RT)}f(\alpha) \quad (2)$$

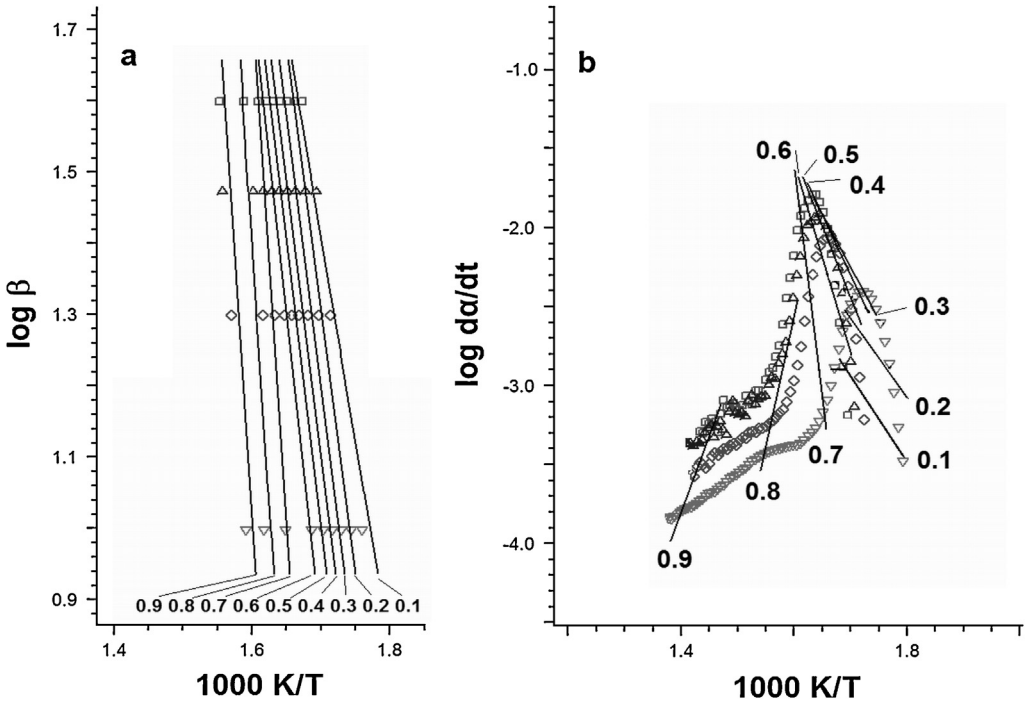

Fig. 4. Plot of log β as a function of 1000/T according to Flynn–Wall–Ozawa method (a) and plot of log dα/dt as a function of 1000/T according to Friedman (b) method for sample Br_P5_Bpy_βCD.

If one takes into account the rate of heating, $\beta = dT/dt$, a new equation of the thermal degradation rate is obtained (Eq. (3)).

$$\frac{d\alpha}{dT} = \frac{A}{\beta} e^{-(E/RT)} f(\alpha) \tag{3}$$

Global kinetic parameters were determined by using Friedman and Flynn–Wall–Ozawa isoconversional methods. These methods use shifts in thermograms with heating rate increase, due to temperature delay as a function of heating rate [26–31].

The Friedman method [32] uses the differential form of the rate equation (Eq. (4)):

$$\ln \frac{d\alpha}{dt} = \ln\ \beta \frac{d\alpha}{dT} = \ln [A f(\alpha)] - \frac{E}{RT} \tag{4}$$

The plot of ln dα/dt versus 1/T, for α = const extracted from the thermograms recorded at different heating rates is a straight line. Activation energy evaluation is undertaken from the slope of the line.

By integrating Eq. (3) between limits T_0 and T_p one obtains the integral function of conversion in Eq. (5), noted $G(\alpha)$.

$$G(\alpha) = \frac{A}{\beta} \int_{T_0}^{T_p} e^{-(E/RT)} dT = \int_0^{\alpha_p} \frac{d\alpha}{f(\alpha)} \tag{5}$$

T_0 represents the initial temperature, corresponding to $\alpha = 0$, and T_p corresponds to the temperature of the peak from DTG curve, where $\alpha = \alpha_p$. The integral function of conversion may reveal insights on the thermal decomposition mechanism [33].

The integral method of Flynn–Wall–Ozawa [34–36] uses the Doyle approximation [37] of the temperature integral given in Eq. (5). The relationship between kinetic parameters and heating rate is given by the following equation:

$$\ln\ \beta = \ln \left(\frac{AE}{R} \right) - \ln\ G(\alpha) - 5.3305 - 1.052 \frac{E}{RT} \tag{6}$$

In order to determine kinetic parameters values with Eq. (6), it was considered that the thermal degradation proscess was described by a first order reaction for $G(\alpha)$. For the same value of α, the plot of ln β as a function of 1/T is a straight line with the slope proportional with the activation energy.

The non-isothermal data extracted from the TGA curves were processed with the software Netzsch Thermokinetics 3. Fig. 4 shows the Flynn–Wall–Ozawa and Friedman plots and Fig. 5 shows the variation of kinetic parameters with conversion degree. Table 2 presents the values of global kinetic parameters determined by applying the two kinetic methods at α values ranging between 0.1 and 0.9 for structure Br_P5_Bpy_βCD. The differences between kinetic parameters values calculated with the two isoconversional methods were explained in the literature [38,39]. The variation of the lines in the Friedman plot and of the kinetic parameters in Fig. 5 confirms the occurring of thermal decomposition process in one main stage [40]. The straight lines from the Flynn–Wall–Ozawa plot in Fig. 4 do not respect the same parallelism throughout the entire thermal decomposition process range, meaning that the assumption of a first order reaction model for $f(\alpha)$ function is not an optimum option.

By analyzing Fig. 5 and Table 2 one may observe that the values of the kinetic parameters increase with the conversion degree,

Table 2
Kinetic parameter values of structure Br_P5_Bpy_βCD calculated with Friedman and Flynn–Wall–Ozawa methods.

α	Kinetic parameters			
	Flynn–Wall–Ozawa		Friedman	
	log A	E (kJ mol^{-1})	log A	E (kJ mol^{-1})
0.1	11.5	106	10.2	93
0.2	13	166	12.2	122
0.3	14	215	13.8	171
0.4	15	265	14.4	220
0.5	15.9	314	15	269
0.6	16.4	364	15.2	318
0.7	17.5	413	19.6	367
0.8	37.5	463	41	416
0.9	68	533	80	515

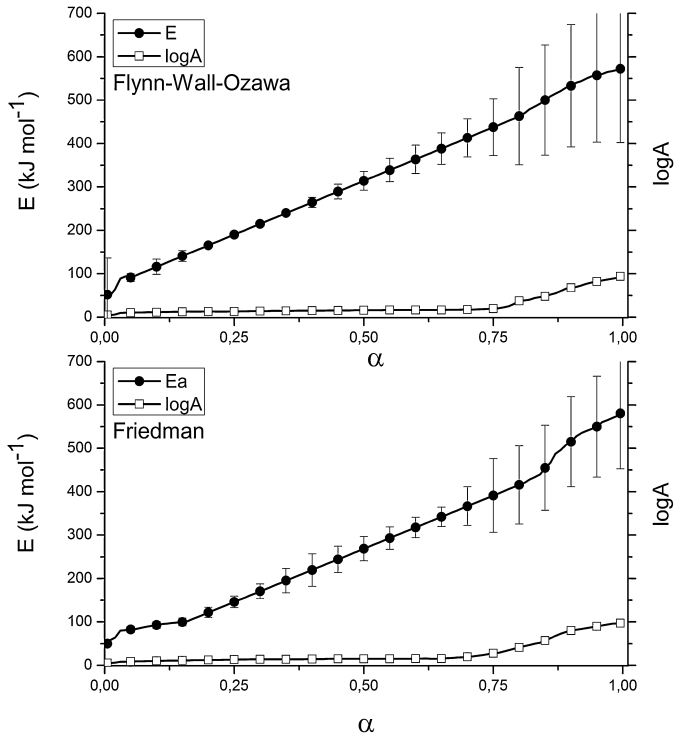

Fig. 5. Variation of kinetic parameters E and $\log A$ with conversion degree for sample Br_P5_Bpy_βCD.

thus suggesting a complex decomposition mechanism *via* successive and/or parallel reactions [41]. In order to determine the kinetic model and the form of the conversion function describing the stage of thermal decomposition for sample Br_P5_Bpy_βCD, a multivariate non-linear regression method was used [41]. All three above mentioned kinetic methods may also be applied for kinetic determinations to some non-degradative thermal processes studied via DSC method [42].

Table 3
Reactions types and corresponding reactions equations, $dr/dt = -A \times \exp(-E/RT) \times f(r,p)$; r—educt concentration; p—solid product concentration.

Code	$f(e,p)$	Reaction type
Fn	r^n	nth—order reaction
Bna	$r^n \times p^a$	Expanded Prout–Tompkins equation (na)
F2	r^2	Second order
D2	$-1/\ln r$	Two dimensional diffusion
D1	$0.5/(1-r)$	One dimensional diffusion
D4	$1.5 \times (r^{-1/3} - 1)$	Three dimensional diffusion (Ginstling–Brounstein type)
D3	$1.5 \times r^{1/3} \times (r^{-1/3} - 1)$	Three dimensional diffusion (Jander's type)
F1	r	First order
R3	$3 \times r^{2/3}$	Three-dimensional phase boundary reaction
A2	$2 \times r \times (-\ln(r))^{1/2}$	Two dimensional nucleation
R2	$2 \times r^{1/2}$	Two dimensional phase boundary reaction
A3	$3 \times r \times (-\ln(r))^{2/3}$	Three dimensional nucleation
An	$n \times r\,(-\ln(r))^{(n-1)/n}$	n-Dimensional nucleation/nucleus growth (Avrami/Erofeev)

Based on the isoconversional data, the software simulated TGA curves by comparison with the experimental ones. 13 reaction types described in the literature and given in Table 3, were tested [27]. Table 4 lists the codes corresponding to the decomposition mechanisms presented in the literature and the statistical parameters (F_{exp} and F_{crit}) which indicate the fit quality of the calculated curves to the experimental ones for sample Br_P5_Bpy_βCD. Through multivariate non-linear regression method there was also possible the determination of the individual kinetic parameters (i.e. corresponding to the DTG curve peak) for the thermal decomposition stage of the studied structure. These values are 242 kJ mol^{-1} for E, 15.23 for $\log A$ and one may observe that they fit within the range of the global kinetic parameters values calculated using the two isoconversional methods and given in Table 2.

Table 4
Non-isothermal kinetic and statistic parameters obtained after non-linear regression through the thermal degradation mechanism of Br_P5_Bpy_βCD in a single step.

Kinetic model	Kinetic parameters	Statistical data		
		Correlation coefficient	F_{crit} (0.95)	F_{exp}
D2	$\log A = 15.23$ E (kJ mol^{-1}) = 242	0.9964080	1.11	1.00
D3	$\log A = 22.37$ E (kJ mol^{-1}) = 289	0.9962605	1.11	1.04
D4	$\log A = 20.77$ E (kJ mol^{-1}) = 272	0.9962397	1.11	1.05
R3	$\log A = 16.6$ E (kJ mol^{-1}) = 70	0.9958820	1.11	1.14
R2	$\log A = 14.9$ E (kJ mol^{-1}) = 285	0.9958205	1.11	1.16
F2	$\log A = 15.74$ E (kJ mol^{-1}) = 202	0.9954410	1.11	1.27
D1	$\log A = 18.85$ E (kJ mol^{-1}) = 216	0.9896657	1.11	2.86
F_n	$\log A = 15.21$ E (kJ mol^{-1}) = 207 $n = 1.7$	0.9882964	1.11	3.24
A2	$\log A = 16.24$ E (kJ mol^{-1}) = 178	0.9862152	1.11	3.81
An	$\log A = 16.7$ E (kJ mol^{-1}) = 191	0.9858430	1.11	3.92
A3	$\log A = 17.67$ E (kJ mol^{-1}) = 197	0.9847897	1.11	4.20
B1	$\log A = 16.1$ E (kJ mol^{-1}) = 213 $n = 1.7$	0.9811923	1.11	5.37
Bna	$\log A = 15.21$ E (kJ mol^{-1}) = 201 $n = 1.8$	0.9789912	1.11	5.51

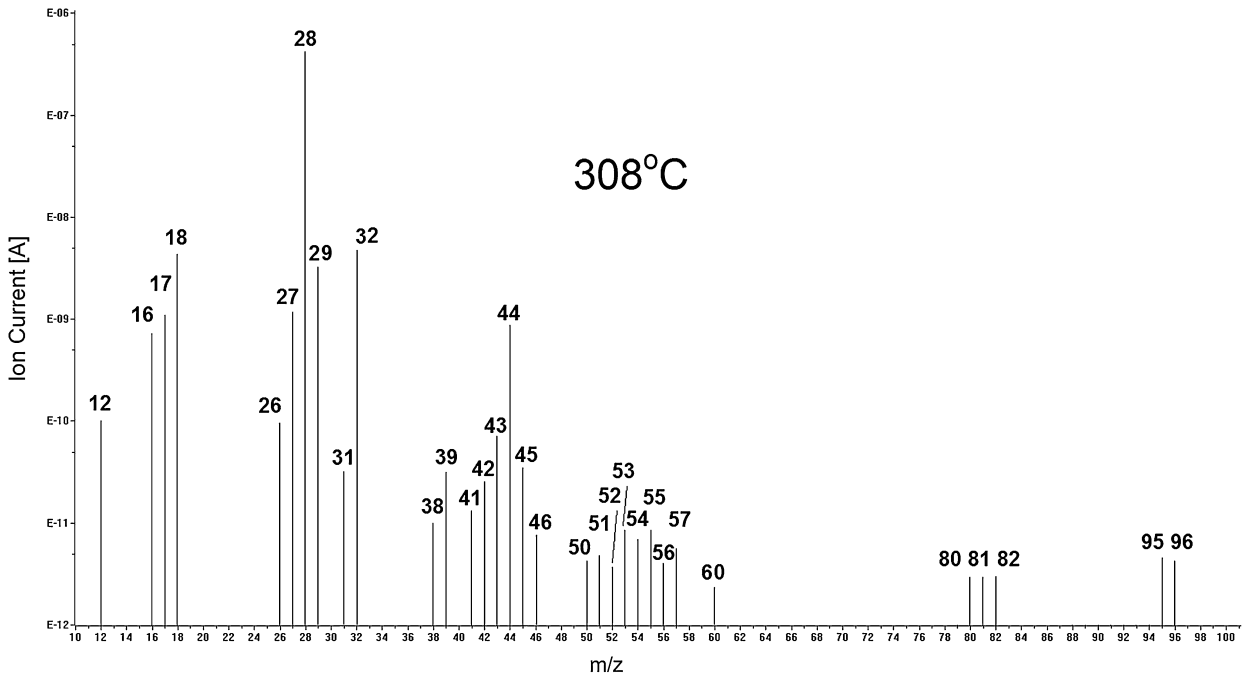

Fig. 6. MS spectrum of structure Br_P5_Bpy_βCD extracted at 308 °C.

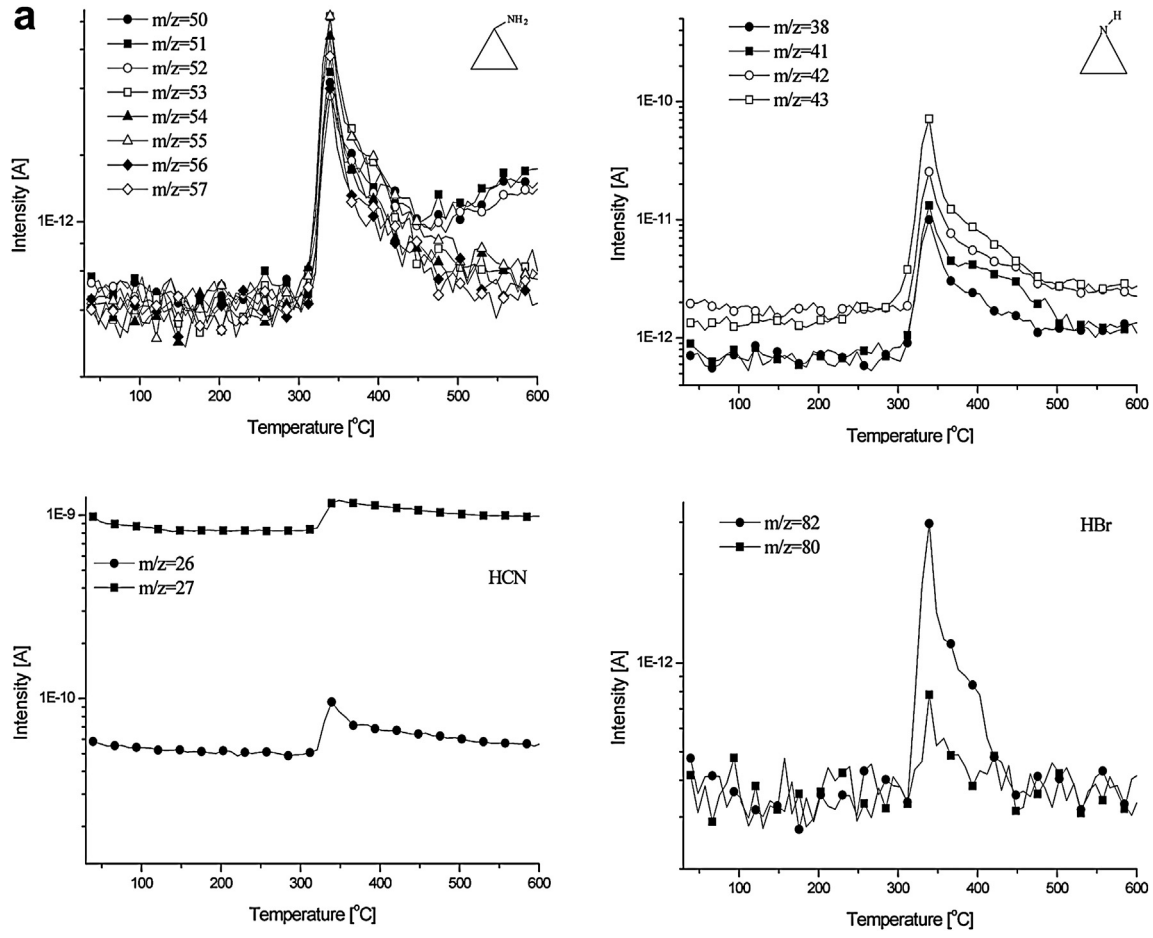

Fig. 7. (a) Ion fragments evolution as a function of temperature in MS spectrum of structure Br_P5_Bpy_βCD.
(b) Ion fragments evolution as a function of temperature in MS spectrum of structure Br_P5_Bpy_βCD.

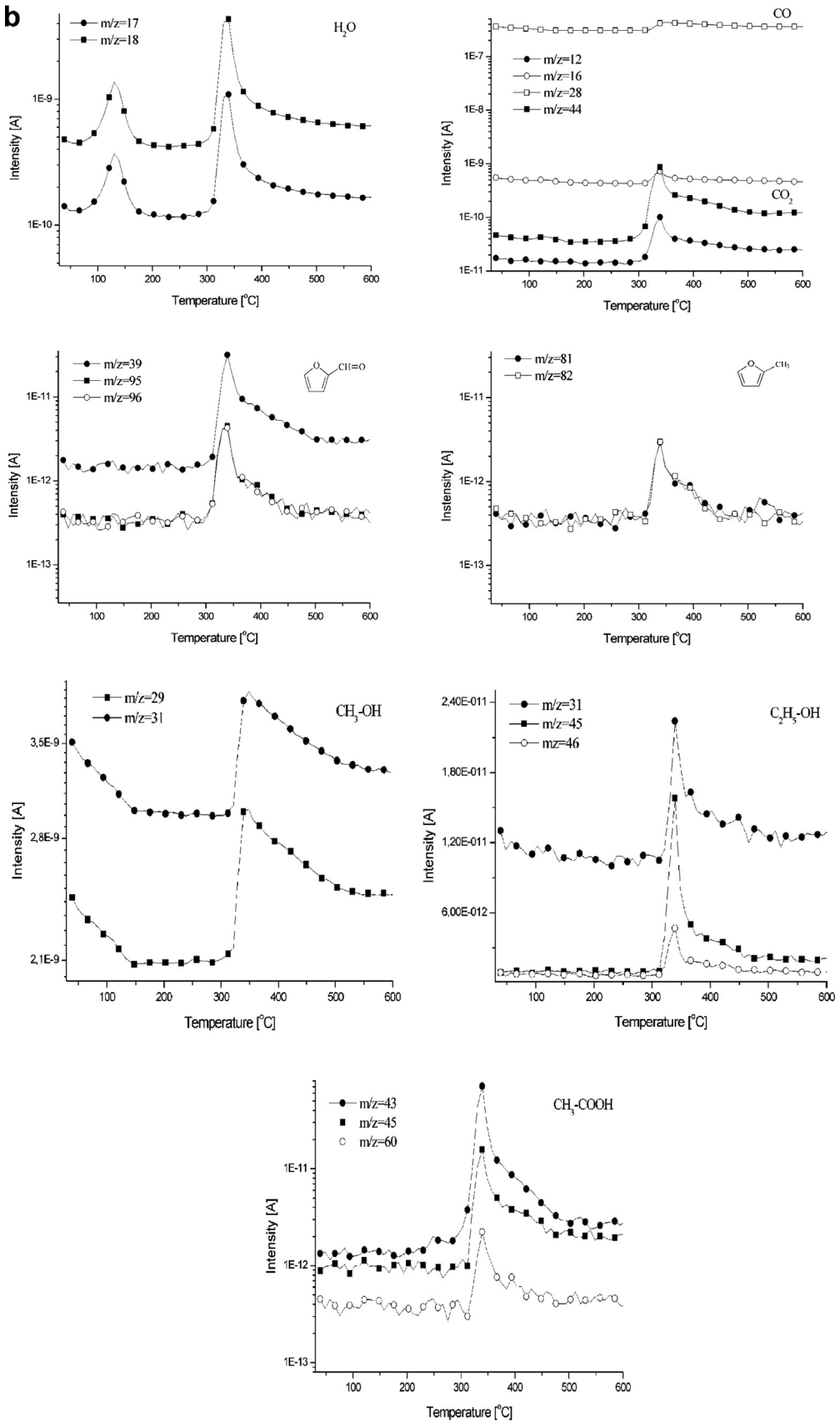

Fig. 7. (*Continued*)

Table 5
Main volatile fragments of Br_P5_Bpy_βCD identified from the MS spectra recorded at 308 °C.

Main fragment *m*/*z*	Molecular weight (g mol^{-1})	Identification	Structure
18, 17	18	Water	H_2O
28, 16	28	Carbon monoxide	CO
44, 12	44	Carbon dioxide	CO_2
27, 26	27	Hydrogen cyanide	HCN
32, 29	32	Methanol	CH_3–OH
46, 45, 31, 39	46	Ethanol	C_2H_5–OH
60, 45, 43	60	Acetic acid	CH_3–COOH
43, 42, 41, 38	43	Ethyleneimine	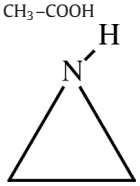
57, 56, 55, 54, 53, 52, 51, 50	57	Cyclopropylamine	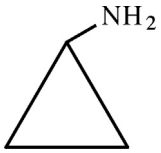
96, 95, 39	96	Furfural	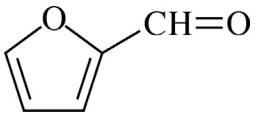
82, 81	82	2-Methyl-furan	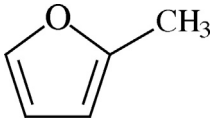
82, 80	80	Hydrogen bromide	HBr

As one may observe from Table 4, the best results were obtained with the two dimensional diffusion (D2) kinetic model for which the software program yielded a correlation coefficient value of 0.9964080, closest to unity. The different diffusion models and their theories are vastly discussed in the literature [40]. A typical situation regarding different diffusion processes is one in which the reaction rate is controlled by the diffusion of a volatilized product into the structure of another participating reactant or product, with respect to changes which may occur in boundary geometry of the reaction(s) interface(s) [40]. Since the DTG curve peak temperature value (308 °C) of the studied complex (Table 1) almost coincides with the theoretical boiling point value of pure Bpy (305 °C), the latter's gaseous molecules may diffuse inwards between the solid degrading βCD structural entities. The thermal decomposition process occurs at the βCD surface with the formation of a charred layer which delays the gaseous evolvement of volatile products entrapped in the βCD cavity. This leads to a diffusion process of the evolved gases through the charred layer, thus hardening mass transfer from the cavity to the exterior and also explaining the increase in thermal decomposition temperatures. Occurrence of a complex thermal decomposition process may also be indicated by the relatively high E values recorded at lower α values (Table 2), correlated with a high $T_{5\%}$ value (295 °C). The increasing in E values with α indicates the hardening of reaction(s) interface(s) advance into the yet unreacted material with temperature increase [40].

3.3. Evolved gas analysis

The NIST Mass Spectral Database was used for the interpretations of mass spectrum of evolved gaseous products. The FTIR–MS analysis of the products generated during the thermal degradation of Br_P5_Bpy_βCD revealed a complex volatile mixture. Fig. 6 shows the MS spectrum of the main gaseous products evolved during thermal decomposition of the studied structure, corresponding to the DTG curve peak (308 °C). Table 5 indicates the *m*/*z* values of the main gaseous fragments.

The presence of water in the gaseous mixture was confirmed by the *m*/*z* values of 18 and 17. Evolvement of CO and CO_2 was demonstrated by *m*/*z* values of 28 and 16 and *m*/*z* values of 44 and 12, respectively. The absence of the fragment *m*/*z* = 14, specific to nitrogen, confirms the correct attribution of ion fragment 28 to CO evolvement. Concerning nitrogen used as purge gas in the analysis, its signal was extracted from the MS spectrum by the device software simultaneously with the background spectrum. The *m*/*z* values of 27 and 26 were attributed to HCN from the guest molecule [20]. The *m*/*z* values of 82 and 80 correspond to HBr traces. Other main gases evolved from the guest molecule consist of ethyleneimine, with *m*/*z* values of 43, 42, 41, 38, and cyclopropylamine, with *m*/*z* values of 57, 56, 55, 54, 53, 52, 51, 50, respectively (Table 5). βCD also exhibited a complex mixture of evolved compounds, such as methanol, with *m*/*z* values of 32, 29, ethanol, with *m*/*z* values 46, 45, 31, and acetic acid, with *m*/*z* values of 60, 45 and 43. Also, there were identified ion fragments corresponding to furfural, with *m*/*z* = 96, 95, 39 and 2-methyl-furan, with *m*/*z* = 82, 81.

Fig. 7a and b shows the evolution of gaseous ion fragments with temperature for the main structural moieties depicted in Table 5. It may be observed that variations of ion fragments exhibit similar evolutions and shapes, thus confirming a correct attribution of signals from the MS spectra.

By analyzing Fig. 7a and b, one may observe that gaseous products containing oxygen, such as water, carbon oxides, acetic acid, furfural, which result during βCD thermal decomposition, evolve at lower temperatures (285–600 °C) compared to the

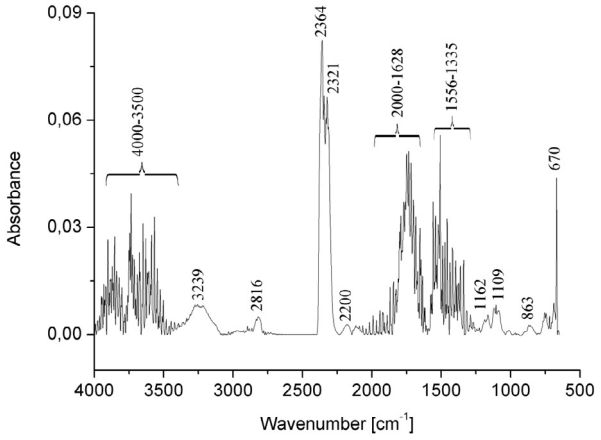

Fig. 8. FTIR spectrum of the evolved gaseous products corresponding to sample Br_P5_Bpy_βCD extracted at 308 °C.

ones containing nitrogen (300–600 °C) and which belong to Bpy (HCN, ethyleneimine, cyclopropylamine). This aspect confirms the mechanism of degradation and mass transfer through diffusion processes.

Fig. 8 shows the FTIR spectrum of the evolved gaseous mixture during thermal degradation of structure Br_P5_Bpy_βCD extracted at 308 °C. The FTIR spectrum confirms the MS spectrum data.

The signals between 4000 and 3500 cm^{-1} correspond to water loss. The large signal in the range 3500–3000 cm^{-1} with a peak at 3239 cm^{-1} corresponds to OH, NH and NH_2 stretching vibrations from alcohols and amine based compounds [43,44]. The absorption band with the peak at 2816 cm^{-1} may be attributed to CH vibration from —CH═O entities [44]. The absorption bands with peaks at 2364, 2321 and 670 cm^{-1} are characteristic to carbon dioxide and the one with the peak at 2200 cm^{-1} to CN group stretching vibration [44]. The signals in the range 1628–2000 cm^{-1} are specific to stretching vibrations of C═O from aldehyde, carboxyl group and C═C entities, which overlap with those of water loss [43]. Similar, the range 1335–1556 cm^{-1} is also specific to overlapping of some absorption bands which characterize stretching vibrations of C═C from furan, water and cycloaliphatic moieties [43,44]. The peak at 863 cm^{-1} may be assigned to C—H stretching vibration from furan derivatives, while peak values of 1162 and 1109 cm^{-1} were attributed to vibrations of C—O—C entities [44].

4. Conclusions

A study on the thermal behavior of a β-cyclodextrin-caged 4,4′-bipyridinium-bis(siloxane) inclusion complex was undertaken. The occurrence of complexation phenomena was evidenced by an increase in the thermal stability of the inclusion complex, compared to that of pure host and guest molecules. Inclusion complex formation was also evidenced through simultaneous TGA–DTA analysis by the lowering in intensity of the guest molecule melting profile and increase in residue mass due to the protection of guest molecule by the cyclodextrin cavity. Non-isothermal degradation kinetic studies were conducted by dynamic thermogravimetry, in nitrogen, up to 700 °C, after recording thermograms at four heating rates. Global kinetic parameters values were determined by means of Friedman and Flynn–Wall–Ozawa isoconversional methods. The kinetic parameters values increased with the conversion degree, indicating a complex thermal decomposition pattern. The kinetic model characterizing the thermal decomposition process and the individual kinetic parameters values were determined by a non-linear multivariate regression method. The thermogravimetric data was best described by a two dimensional diffusion (D2) kinetic model. The main volatile compounds evolved during thermal degradation were: water, carbon monoxide, carbon dioxide, hydrogen cyanide, methanol and ethanol, acetic acid, hydrogen bromide and amine and furan derivatives.

Acknowledgments

Authors acknowledge the financial support of two grants of the National Authority for Scientific Research, CNCS-UEFISCDI, project numbers: PNII-ID-PCCE-2011-2-0028 and PN-II-ID-PCE-2011-3-0187. Authors are grateful to Dr. Nita Tudorachi of the “Petru Poni” Institute of Macromolecular Chemistry in Iasi, Romania, for the coupled TG–FTIR–MS measurements.

References

[1] M. Irimia, G. Lisa, R. Danac, N. Aelenei, I. Druta, Physico-chemical characterization of some diquaternary salts of 4,4′-bipyridine, Croat. Chem. Acta 77 (4) (2004) 587–591.
[2] N. Marangoci, S.S. Maier, R. Ardeleanu, A. Arvinte, A. Fifere, A.C. Petrovici, A. Nicolescu, V. Nastasa, M. Mares, S.A. Pasca, R.F. Moraru, M. Pinteala, A. Chiriac, Low toxicity β-cyclodextrin-caged 4,4′-bipyridinium-bis(siloxane): synthesis and evaluation, Chem. Res. Toxicol. 27 (2014) 546–557.
[3] Z. Shi, K.G. Neoh, E.T. Kang, Antibacterial activity of polymeric substrate with surface grafted viologen moieties, Biomaterials 26 (2005) 501–508.
[4] M.E. Nuñez, B.D. Hall, J.K. Barton, Long-range oxidative damage of DNA: effects of distance and sequence, Chem. Biol. 6 (1999) 85–97.
[5] L. Michaelis, E.S. Hill, The viologen indicators, J. Gen. Physiol. 16 (1933) 859–873.
[6] R.J. Dinis-Oliveira, J.A. Duarte, A. Sánchez-Navarro, F. Remião, M.L. Bastos, F. Carvalho, Paraquat poisonings: mechanisms of lung toxicity, clinical features, and treatment, Crit. Rev. Toxicol. 38 (2008) 13–71.
[7] G. Zweig, N. Shavit, M. Avron, Diquat (1,1-ethylene-2,2′-dipyridylium dibromide) in photo-reactions of isolated chloroplasts, Biochim. Biophys. Acta 109 (1965) 332–346.
[8] A.D. Dodge, The mode of action of the bipyridylium herbicides, paraquat and diquat, Endeavour 30 (1971) 130–135.
[9] J.M. Hatcher, K.D. Pennell, M.W. Miller, Parkinson's disease and pesticides: a toxicological perspective, Trends Pharmacol. Sci. 29 (2008) 322–329.
[10] K. Wang, D.S. Guo, H.Q. Zhang, D. Li, X.L. Zheng, Y. Liu, Highly effective binding of viologens by *p*-sulfonatocalixarenes for the treatment of viologen poisoning, J. Med. Chem. 52 (2009) 6402–6412.
[11] C. Folch-Cano, M. Yazdani-Pedram, C. Olea-Azar, Inclusion and functionalization of polymers with cyclodextrins: current applications and future prospects, Molecules 19 (2014) 14066–14079.
[12] F. Abbasi, H. Mirzadeh, A.A. Katbab, Modification of polysiloxane polymers for biomedical applications: a review, Polym. Int. 50 (2001) 1279–1287.
[13] Y. Andriani, I.C. Morrow, E. Taran, G.A. Edwards, T.L. Schiller, A.F. Osman, J. Darren, D.J. Martin, In vitro biostability of poly(dimethyl siloxane/hexamethylene oxide)-based polyurethane/layered silicate nanocomposites, Acta Biomater. 9 (2013) 8308–8317.
[14] L.X. Song, C.F. Teng, P. Xu, H.M. Wang, Z.Q. Zhang, Q.Q. Liu, Thermal decomposition behaviors of β-cyclodextrin, its inclusion complexes of alkyl amines, and complexed β-cyclodextrin at different heating rates, J. Inclusion Phenom. Macrocyclic Chem. 60 (2008) 223–233.
[15] P. Xu, L.-X. Song, Thermal decomposition kinetics of survived β-cyclodextrin from an inclusion complex of β-cyclodextrin with clove oil, Acta Phys.—Chim. Sin. 24 (2008) 2214–2220.
[16] G.E. Zhang, X.T. Li, S.J. Tan, J.H. Li, J.Y. Wang, X.D. Lou, Q.T. Cheng, Kinetic studies on the thermal dissociation of β-cyclodextrin-ethyl benzoate inclusion complexes, J. Therm. Anal. Calorim. 54 (1998) 947–956.
[17] A. Corciova, C. Ciobanu, A. Poiata, C. Mircea, A. Nicolescu, M. Drobota, C.-D. Varganici, T. Pinteala, N. Marangoci, Antibacterial and antioxidant properties of hesperidin: β-cyclodextrin complexes obtained by different techniques, J. Inclusion Phenom. Macrocyclic Chem. 81 (2015) 71–84.
[18] A. Corciova, C. Ciobanu, A. Poiata, A. Nicolescu, M. Drobota, C.-D. Varganici, T. Pinteala, A. Fifere, N. Marangoci, C. Mircea, Inclusion complexes of hesperidin with hydroxypropyl-β-cyclodextrin. Physico-chemical characterization and biological assessment, Dig. J. Nanomater. Biostruct. 9 (4) (2014) 1623–1637.
[19] N. Marangoci, M. Mares, M. Silion, A. Fifere, C. Varganici, A. Nicolescu, C. Deleanu, A. Coroaba, M. Pinteala, B.C. Simionescu, Inclusion complex of a new propiconazole derivative with β-cyclodextrin: NMR, ESI–MS and preliminary pharmacological studies, Res. Pharm. Sci. 1 (2011) 27–37.
[20] D. Czakis-Sulikowska, J. Radwańska-Doczekalska, M. Markiewicz, M. Pietrzak, Thermal characterization of new complexes of Zn(II) and Cd(II) with some bipyridine isomers and propionates, J. Therm. Anal. Calorim. 93 (3) (2008) 789–794.
[21] F. Trotta, M. Zanetti, G. Camino, Thermal degradation of cyclodextrins, Polym. Degrad. Stab. 69 (3) (2000) 373–379.
[22] J.E. Mark, Polymer Data Handbook, Oxford University Press, Oxford, 1999.

[23] M. Spulber, M. Pinteala, A. Fifere, V. Harabagiu, B.C. Simionescu, Inclusion complexes of 5-flucytosine with β-cyclodextrin and hydroxypropyl-β-cyclodextrin: characterization in aqueous solution and in solid state, J. Inclusion Phenom. Macrocyclic Chem. 62 (2008) 117–125.
[24] T. Loftsson, D. Hreinsdottir, M. Masson, Evaluation of cyclodextrin solubilization of drugs, Int. J. Pharm. 302 (2005) 18–28.
[25] F. Taneri, G. Taner, Z. Aigner, M.K. Taneri, MK, Improvement in the physicochemical properties of ketoconazole through complexation with cyclodextrin derivatives, J. Inclusion Phenom. Macrocyclic Chem. 44 (2002) 257–260.
[26] D. Rosu, N. Tudorachi, L. Rosu, Investigations on the thermal stability of a MDI based polyurethane elastomer, J. Anal. Appl. Pyrol. 89 (2010) 152–158.
[27] D. Rosu, L. Rosu, M. Brebu, Thermal stability of silver sulfathiazole–epoxy resin network, J. Anal. Appl. Pyrol. 92 (2011) 10–18.
[28] C.-D. Varganici, A. Durdureanu-Angheluta, D. Rosu, M. Pinteala, B.C. Simionescu, Thermal degradation of magnetite nanoparticles with hydrophilic shell, J. Anal. Appl. Pyrol. 96 (2012) 63–68.
[29] D. Rosu, L. Rosu, C.-D. Varganici, The thermal stability of some semi-interpenetrated polymer networks based on epoxy resin and aromatic polyurethane, J. Anal. Appl. Pyrol. 100 (2013) 103–110.
[30] C.-D. Varganici, O.M. Paduraru, L. Rosu, D. Rosu, B.C. Simionescu, Thermal stability of some cryogels based on poly(vinyl alcohol) and cellulose, J. Anal. Appl. Pyrol. 104 (2013) 77–83.
[31] C.-D. Varganici, D. Rosu, C. Barbu-Mic, L. Rosu, D. Popovici, C. Hulubei, B.C. Simionescu, On the thermal stability of some aromatic–aliphatic polyimides, J. Anal. Appl. Pyrol. 113 (2015) 390–401.
[32] S. Vyazovkin, A.K. Burnham, J.M. Criado Luque, L.A. Pérez-Maqueda, C. Popescu, N. Sbirrazoulli, ICTAC Kinetics Committee recommendations for performing kinetic computations on thermal analysis data, Thermochim. Acta 520 (2011) 1–19.
[33] M. Villanueva, J.L. Martin-Iglesias, J.A. Rodriguez-Anon, J. Proupin-Castineiras, Thermal study of an epoxy system DGEBA ($n = 0$) MXDA modified with POSS, J. Therm. Anal. Calorim. 96 (2009) 575–582.
[34] J. Opfermann, E. Kaisersberger, An advantageous variant of the Ozawa–Flynn–Wall analysis, Thermochim. Acta 203 (1992) 167–175.
[35] T. Ozawa, A new method of analysing thermogravimetric data, Bull. Chem. Soc. Jpn. 38 (1965) 1881–1886.
[36] J.H. Flynn, L.A. Wall, A quick, direct method for the determination of activation energy from thermogravimetric data, J. Polym. Sci., B: Polym. Lett. 4 (1966) 323–328.
[37] C.D. Doyle, Estimating isothermal life from thermogravimetric data, J. Appl. Polym. Sci. 6 (1962) 639–642.
[38] P. Budrugeac, E. Segal, Some methodological problems concerning nonisothermal kinetic analysis of heterogeneous solid–gas reactions, Int. J. Chem. Kinet. 33 (2001) 564–573.
[39] P. Budrugeac, D. Homentcovschi, E. Segal, Critical analysis of the isoconversional methods for evaluating the activation energy. I. Theoretical background, J. Therm. Anal. Calorim. 63 (2001) 457–463.
[40] A.K. Galwey, M.E. Brown, Kinetic background to thermal analysis and calorimetry, in: M.E. Brown (Ed.), Handbook of Thermal Analysis and Calorimetry, Elsevier Science, Amsterdam, 1998, pp. 150–205.
[41] J. Opferman, Kinetic analysis using multivariate non-linear regression, J. Therm. Anal. Calorim. 60 (2000) 641–658.
[42] C.-D. Varganici, O. Ursache, C. Gaina, V. Gaina, B.C. Simionescu, Studies on new hybrid materials prepared by both Diels–Alder and Michael addition reactions, J. Therm. Anal. Calorim. 111 (2) (2013) 1561–1570.
[43] R.M. Silverstein, F.X. Webster, D.J. Kiemle, Spectrometric Identification of Organic Compounds, Wiley, New York, NY, 2005, pp. 87.
[44] A.T. Balaban, M. Banciu, I. Pogany, Applications of Physical Methods in Organic Chemistry, Scientific and Encyclopedic Publishers, Bucharest, 1983.